First Demonstration of Improved Yield with reduced Adiabat in Inertial Confinement Fusion Implosions on the National Ignition Facility

M. Hohenberger,[1, a)] D. S. Clark,[1] K. D. Humbird,[1] A. Pak,[1] A. Do,[1] C. V. Young,[1] T. Döppner,[1] A. L. Kritcher,[1] D. T. Casey,[1] A. Allen,[2] S. H. Baxamusa,[1] B. Bachmann,[1] J. Biener,[1] R. M. Bionta,[1] T. Braun,[1] T. M. Briggs,[1] T. Chapman,[1] C. R. Danly,[3] T. R. Dittrich,[1] L. Divol,[1] M. Durocher,[3] V. E. Fatherley,[3] T. Fehrenbach,[4] M. Freeman,[3] M. Gatu Johnson,[5] S. W. Haan,[1] K. D. Hahn,[1] S. Hayes,[1] O. A. Hurricane,[1] S. F. Khan,[1] C. W. Kong,[2] B. Kozioziemski,[1] O. L. Landen,[1] B. J. MacGowan,[1] S. A. MacLaren,[1] M. Millot,[1] A. S. Moore,[1] A. Nikroo,[1] R. C. Nora,[1] J. E. Ralph,[1] M. Ratledge,[2] M. S. Rubery,[3] G. Saavedra,[3] D. J. Schlossberg,[1] M. P. Selwood,[1] M. Stadermann,[1] S. Stoupin,[1] R. Tommasini,[1] C. Trosseille,[1] C. R. Weber,[1] C. Wild,[4] C. Wilde,[3] B. T. Wolfe,[3] B. N. Woodworth,[1] and A. B. Zylstra[1, b)]

[1)] *Lawrence Livermore National Laboratory, P.O. Box 808, Livermore, California 94551-0808, USA*

[2)] *General Atomics, P.O. Box 85608, San Diego, California 92186-5608, USA*

[3)] *Los Alamos National Laboratory, Mail Stop F663, Los Alamos, New Mexico 87545, USA*

[4)] *Diamond Materials GmbH, 79108 Freiburg, Germany*

[5)] *Massachusetts Institute of Technology, Cambridge, Massachusetts 02139, USA*

(Dated: 5 November 2025)

Laser-driven, indirect-drive inertial confinement fusion (ICF) experiments at the National Ignition Facility (NIF) recently achieved a target gain greater than one, where fusion energy output exceeds input laser energy [Abu-Shawareb et al., Phys. Rev. Lett. 132, 065102 (2024)]. Despite this milestone, gain levels remain insufficient for practical applications such as inertial fusion energy, making performance improvement critical. One promising approach is increasing fuel compression by lowering the implosion adiabat. To explore reduced adiabat, experiments were conducted modifying the laser pulse shape and shock timing of an existing 1.9-MJ-drive implosion design performing near the ignition cliff [Abu-Shawareb et al., Phys. Rev. Lett. 129, 075001 (2022)]. These experiments demonstrated increased compression and fusion yield in ICF implosions at the NIF by using a lower fuel adiabat, and increased compression with a reduced adiabat in high-density carbon ablators. The updated design achieved up to 80% higher fusion yield and 14% greater fuel compression compared to the previous best-performing 1.9-MJ experiment, with repeatable performance, and is the only implosion design to achieve a target gain exceeding one with <2.04 MJ laser energy. Notably, this work was made possible because of recent advances in target quality and pulse shape control allowing experimental access to the ignition regime, and thereby increased sensitivity to adiabat. This work addresses a longstanding question in ICF research and lays the foundation for higher target gains through optimized implosion strategies. It underscore the potential of reduced adiabat designs to enhance compression and fusion yields for future ICF applications.

I. INTRODUCTION

In indirect-drive, inertial-confinement fusion experiments performed at the National Ignition Facility (NIF),[1] cryogenic deuterium-tritium (DT) fuel is rapidly and symmetrically compressed to the high temperatures and densities required for fusion reactions to occur.[2–4] The DT fuel is contained as a cryogenic layer inside a thin-wall, high-density carbon (HDC) capsule. This capsule is placed at the center of a cylindrical, high-Z cavity (hohlraum), typically made of gold and/or uranium. The compression drive is provided by 192 high-power, 351-nm lasers depositing their energy of up to 2.2 MJ inside the hohlraum. Through interaction with the hohlraum walls, the incident laser energy is converted into a nearly uniform, quasi-thermal x-ray bath of ∼300 eV, that drives the capsule implosion with a velocity of v_{imp} ∼400 km/s through ablation of the outer capsule material, thus accelerating the remaining ablator and DT fuel inward. Upon stagnation, the kinetic energy of the implosion has been converted into internal energy, creating a high-density shell of DT fuel, surrounding a lower-density but higher-temperature, central hot spot of DT plasma, with conditions sufficient for fusion reactions to occur, D+T → ^{4}He (3.5 MeV) + n (14.1 MeV). In a sufficiently confined, fast and uniform implosion, the α-particles released in these reactions then deposit their energy in the assembled fuel via collisions, providing additional heating. If the energy deposition from α-heating exceeds the plasma power losses, the Lawson criterion for ignition is satisfied, and the additional heating launches a wave of fusion reactions through the fuel. This releases more energy via fusion reactions than initially used to start the experiment, thereby achieving ignition and target gain $G = E_{out}/E_{in} > 1$, and further boosting the hot-spot

[a)] corresponding author: hohenberger1@llnl.gov

[b)] Current address: Pacific Fusion, Palo Alto, California 94306, USA

temperature. This milestone was recently demonstrated experimentally on the NIF for the first time and after decades of research,[5] thus achieving one of the NIF's primary goals.

Since then fusion ignition has been demonstrated repeatedly, with current designs achieving G $\gtrsim$ 1.[5] However, future applications will require target gains >15, and a major challenge is to improve performance further. Multiple routes are being considered, which can roughly be categorized by improvements to the driver (increased laser energy and/or peak power), improved coupling (reduced hohlraum losses, increased laser to x-ray conversion, or coupling of x-rays to the capsule), and increased fuel areal density, ρR.[6]

The latter has long been suggested by both modeling and theory as a significant lever on fusion output. The impact of increased fuel compression on an igniting implosion is two-fold. First, it increases the rate of PdV work done on the central hot spot and the resulting fusion yield in the absence of α-particle self-heating, $Y_{no-\alpha}$. Second, it increases the areal density of the confining fuel, allowing for increased fuel burn fractions and higher yield amplification, Y_{amp}. The impact of increasing compression can be estimated via a simplified 1D implosion model.[7] Assuming current-design implosions ($\rho R_{no-\alpha} \approx 1.2$ g/cm^2) near the ignition cliff, and with otherwise identical design parameters (e.g., fuel mass, implosion velocity, etc.), the total yield can be expressed in 1D in terms of the peak, no-α areal density $\rho R_{no-\alpha}$, i.e., assuming the areal density is not affected by any yield amplification. As will be discussed below, significant levels of neutron yield lower the experimentally observable ρR compared to its $\rho R_{no-\alpha}$ value.

$$Y_{total} = Y_{no-\alpha} \times Y_{amp} \sim \rho R_{no-\alpha}^{1.5} \times \left(\rho R_{no-\alpha}^{1.9}\right)^{\eta}. \quad (1)$$

The quantity η increases with yield amplification, scaling from η=0.5 in moderately burning plasmas with $1.5 < Y_{amp} < 2$, up to η=5 for $Y_{amp} > 8$ and the designs of interest here.[7] It follows that the 1D yield scales as $Y \sim \rho R_{no-\alpha}^{11}$, corresponding to a doubling of the total yield for a ∼7% increase in compression, and emphasizing its strong lever on performance in igniting implosion designs. However, it should be noted that the strong dependence on areal density in Eq. 1 is expected to roll over for implosions beyond the ignition cliff because of fuel depletion limiting the burn-up fraction. It also ignores, e.g., a strong dependence on implosion velocity, or impacts from small changes to drive asymmetry between designs, affecting the energy coupling to the stagnated hot spot and fuel. Notably, the impact of such degradations becomes more pronounced at increasing levels of Y_{amp}, and as such the simplified $\rho R_{no-\alpha}^{11}$ scaling is not expected to be observed experimentally.

Increased areal density is a key motivation behind the efforts to increase the NIF's available laser energy beyond its initial design envelope of 1.8 MJ. The increase in laser energy allows for a thicker ablator, and therefore an increased piston and resulting compression.[6] Notably, this strategy ultimately achieved ignition and G>1 with a laser energy of 2.05 MJ.[5,8,9] In contrast, this paper reports on a parallel effort to improve compression via modifications to the implosion design *without* increasing the incident laser energy.

The figure of merit for fuel compression is the in-flight adiabat, α_{if}, a measure of the fuel's entropy and defined as the ratio of the fuel pressure to the Fermi degenerate pressure at peak implosion velocity.[10] It correlates positively with the theoretical minimum energy required for ignition,[11] and inversely relates to the fuel's areal density at stagnation, $\rho R \sim \alpha_{if}^{-0.6}$, where, based on 1D simulations and analytic derivations, the power-law dependence can range from approximately 0.5 to 1 for adiabats spanning ∼2 to 4.[6,12] In NIF indirect-drive implosions, α_{if} is controlled via the incident laser pulse shape that drives the target compression. It typically comprises a sequence of three shocks to compress the fuel before acceleration at peak power and to set the in-flight adiabat. To limit entropy buildup and maintain a low α_{if}, shocks are typically timed to merge close to the inner surface of the DT-fuel ice layer, just before breaking out into the gas-filled hot spot. Thus, controlling the shock strength and relative spacing introduces changes to the fuel's adiabat and compressibility. However, in contrast to analytical considerations, experimental performance has historically not benefitted from reducing the adiabat.[13] This has been observed in indirect-drive designs with both CH[14,15] and HDC[16] ablators, or in direct-drive implosions.[17] This was attributed to the growth of hydrodynamic instabilities seeded by capsule imperfections, or engineering features such as the tent supporting the capsule, and the fill tube.[18–22] Indeed, *increasing* the adiabat and trading compressibility in favor of stability, has resulted in significant performance boosts for both indirect- and direct-drive designs.[23–25]

In this paper, we report on experiments in the *Shock-Merge* (SM) campaign which, for the first time, demonstrate enhanced fusion yields and increased observed compression for an ICF implosion as a result of a decreased design adiabat, and with repeatable performance, consistent with design expectations. For a fixed laser energy of 1.9 MJ, these experiments demonstrated increased areal density of 14% and greater fusion yields of up to 80% than experiments with higher design adiabats, thereby answering a long-standing question in ICF sciences. Furthermore, it is the only design to have achieved G>1 with a laser energy <2.04 MJ, thus setting a new, lower record for the energy required to achieve ignition.

This paper is organized as follows. Section II provides a brief overview of the experimental design and its implementation. Section III discusses key experimental data to assess the impact of these changes on compression and performance. Finally, Section IV summarizes the results and presents the conclusions.

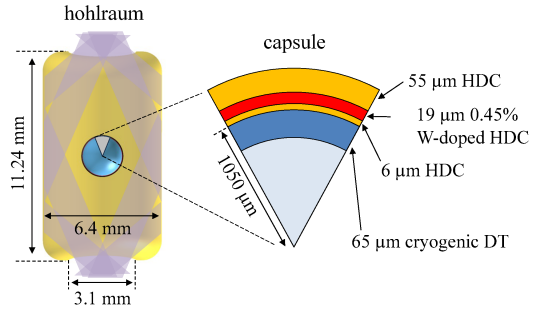

FIG. 1. Schematic of the HyE and SM target design. A 11.24 × 6.4-mm hohlraum converts the incident laser energy to x-rays to implode a High Density Carbon (HDC) capsule with 1130 μm outer radius, 80 μm thick wall, and a 65 μm cryogenic DT fuel layer. To control high-energy x-ray pre-heating, the capsule includes a 19 μm thick, 0.45 at.% tungsten-doped layer, that is offset by 6 μm from the shell inner surface.

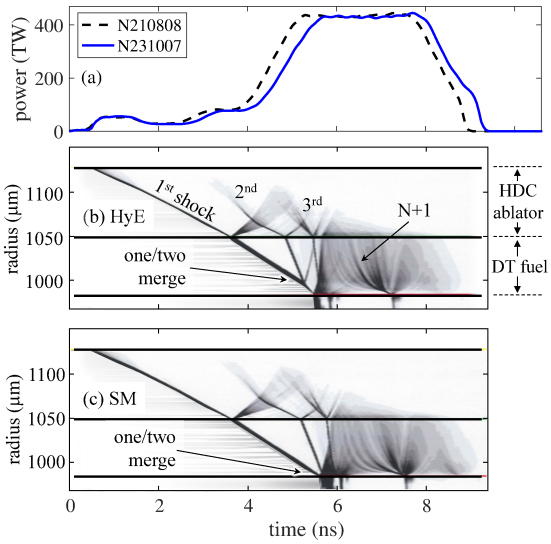

FIG. 2. (Color online) (a) The laser pulse for the SM design (experiment N231007, blue) features a delayed second shock at 3 ns, and a slowed rise to peak power between 4 to 5 ns compared to the reference HyE design (experiment N210808, black dashed). (b) and (c) show the calculated shock propagation for both HyE and SM, respectively. The updated shock timing for SM delays the one/two shock merge to the ice-gas interface, and weakens the N+1 shock strength for an overall reduction of the inflight adiabat.

II. EXPERIMENTAL DESIGN

The experiments discussed in this paper are based on an updated design of NIF experiment N210808. NIF experiments are identified via the letter N followed by six digits denoting the experiment's start date in the format year (YY), month (MM), and day (DD). An overview of the experimental and computational design underpinning N210808 can be found in Refs. [26–28]. Importantly, N210808 is the best-performing experiment in the 1.9-MJ *Hybrid-E* (HyE) series, it was the first ICF implosion to achieve >1 MJ of nuclear yield, and, with G=0.7, the first to achieve a target gain approaching unity. Its design and robustness were studied extensively through multiple repeat attempts, although none surpassed its performance due to a combination of unintentional variations to laser delivery and target quality.[29]

A schematic of the hohlraum and target dimensions for both HyE and SM is shown in Fig. 1. Both campaigns used a 11.24 × 6.4-mm cylindrical hohlraum, with 3.1-mm diameter laser entrance holes. Capsules nominally comprised a 1050-μm inner radius, and a 80-μm thick ablator with a 19 μm buried layer doped with 0.45 at.% tungsten, as well as a 65-μm cryogenic-DT fuel layer. The key difference between the reference HyE design and SM is illustrated in Fig. 2(a), showing the pulse shape for N210808 (black, dashed line) compared to the SM pulse shape from experiment N231007 (blue). Figures 2(b) and (c) show 1D radiation-hydrodynamics calculations (HYDRA)[30] of the shock propagation inside the target for HyE and SM, respectively. Here, the solid, horizontal lines mark the outer (1130 μm), and inner (1050 μm) HDC wall radius, as well as the inner DT ice radius (985 μm), respectively. The plots show the three, laser-driven shocks launched at 0.5, 3, and 5 ns, respectively. In addition, the simulations show the various shocks launched via reflections at the material boundaries, including the so-called N+1 shock caused by the rarefaction wave from the first shock breakout reflecting on the ablation front, and traveling back to the target center. In the HyE design on N210808, shocks one and two merged ∼52 μm into the 65-μm ice layer, or ∼13 μm from the inner surface, as labeled with the arrow in Fig. 2(b). This deliberate design choice locally increased the innermost fuel-layer's adiabat as a result of the stronger, coalesced one/two shock. In contrast to 1D predictions, this had proven a successful strategy for performance optimization in previous experiments.[27] For the lower-adiabat, SM design, two changes were introduced to the pulse shape. Firstly, the second shock was shifted later by 200 ps, delaying the one/two shock merge to the ice/gas interface at 985 μm. Secondly, the rise to peak power between ∼4 to 5 ns was stretched out by an additional 200 ps to weaken the N+1 shock strength and reduce its impact on the fuel's pressure and adiabat.

Note that the longer pulse shape makes symmetry control more challenging. As the hohlraum-wall plasma expands into the hohlraum volume, it blocks off laser beam propagation to the target waist, thus reducing equatorial drive onto the capsule.[31–33] This is further exacerbated by extending the pulse width. The longer SM pulse shape causes a drop of equatorial capsule drive late in the implosion, and a negative P_2 amplitude at stagnation compared to the round N210808 implosion. To offset the loss in equatorial drive, the wavelength separation, $\Delta\lambda$, between inner and outer beams was increased from 1.8Å to 2.7Å. Here, inner and outer refers to beams

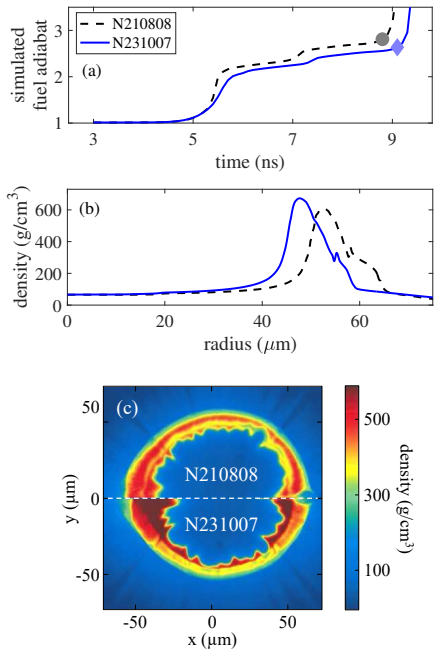

FIG. 3. (Color online) 1D simulations with the updated SM pulse shape for experiment N231007 (blue) compared to HyE experiment N210808 (black, dashed) show (a) a reduced fuel adiabat, and (b) an increased peak density and higher convergence at stagnation. (c) 2D simulated density profiles are consistent with the 1D findings.

focused either near the hohlraum waist (inner) or near the upper and lower ends of the hohlraum cavity (outer). The wavelength separation controls cross-beam energy transfer, with higher $\Delta\lambda$ increasing the energy directed to the hohlraum waist.[34] Importantly, the shock-timing and wavelength shift were the only deliberate changes between N210808 and the SM design. As the wavelength shift is a necessary change introduced to recover a round hot spot, this leaves the pulse-shape change, and the resulting lower adiabat, as the key difference between HyE and SM. All other parameters (e.g., target details, laser energy, etc.) were kept identical.

Compression on DT-fueled experiments is inferred via the downscattered ratio (DSR). This is the ratio of neutrons downscattered to 10-12 MeV by the dense fuel surrounding the hot spot, relative to the primary neutron yield in the energy range of 13-15 MeV.[35] It scales with the areal density as $\rho R[\mathrm{g/cm^2}]\approx 0.18\times \mathrm{DSR}[\%]$, and thus changes in compression directly translate to the observed DSR.[36] Note that quoted DSR's refer to the solid-angle averaged value as introduced in Ref. 37.

The simulated impact of the updated pulse shape on implosion dynamics is shown in Fig. 3. Simulations were originally tuned to the HyE / N210808 data, and then applied to the SM experiments with the updated pulse shapes, and with no other changes (e.g., multipliers, etc.). The fuel-averaged adiabat from 1D simulations plotted in Fig. 3(a) for the SM design (blue, solid line) is noticeably reduced compared to HyE (black, dashed line). The time of peak implosion velocity is highlighted in Fig. 3(a) by the data points, giving calculated adiabats of 2.89 and 2.68 for the HyE and SM implosions, respectively. This results in both increased convergence and peak density at stagnation for SM, as shown in Fig. 3(b).

In these 1D simulations, the fuel ρR increases by 11%, with a calculated $\mathrm{DSR}_{no-\alpha}$, i.e., the DSR in the absence of α-particle heating, of 4.39% and 4.88% for HyE and SM, respectively. This increase is stronger than expected from the simple $\rho R \sim \alpha_{if}^{-0.6}$ scaling. Though, it should be noted that α_{if} is typically defined as a mass-averaged quantity, whereas the HyE shock timing introduces a significant adiabat gradient near the fuel-gas interface, that is not captured by a simple mass-averaging. The delayed one/two shock merge affects the fuel adiabat only in the innermost 13 μm, whereas the fuel at larger radii is not impacted.

In the simulations, the adiabat reduction, and the resulting DSR increase, have approximately equal contributions from the delayed one/two merge, and the reduced N+1 shock strength. Additionally, the extended pulse comes at a small cost in simulated implosion velocity of ∼1%, as the delayed peak power acts on a further imploded capsule with reduced surface area and laser-to-capsule coupling. The calculated 1-D yields are $Y_{HyE} = 1.5\times10^{18}$ and $Y_{SM} = 2.0\times10^{18}$. Results from 2D calculations of the two designs can be seen in Fig. 3(c), showing mass density profiles at stagnation for HyE (top half) and SM (bottom half), respectively. The data show qualitatively similar results to the 1D simulations, with the SM calculation reaching both higher convergence and increased peak densities. Compared to the 1D calculations, these simulations predict a larger impact of the updated pulse shape, with calculated no-α DSR's of 4.23% vs 4.99%, and calculated total yields of $Y_{HyE} = 0.5\times10^{18}$ and $Y_{SM} = 2.2\times10^{18}$. Interestingly, the 2D yield result for SM is consistent with the corresponding 1D calculation, while the HyE result drops by a factor three.

III. EXPERIMENTAL DATA AND DISCUSSION

Dedicated shock-timing measurements experimentally confirmed that the updated pulse shape has the desired impact on the shock dynamics. In these experiments, a diagnostic cone is added to the hohlraum target, penetrating both the hohlraum and capsule walls. Additionally, the standard DT-ice fuel is replaced with liquid deuterium, which fills both the capsule and cone.[38] The laser-driven shocks propagating through the fill form a highly reflective shock front which can be tracked via interferometry using the VISAR diagnostic.[39,40] Results from these measurements are shown in Figs. 4(a) and (b), which plot both measured (solid line) and calculated (dashed line) shock velocities as a function of time for the HyE and SM designs, respectively. As can be seen, experimental data and simulation results are in good agree-

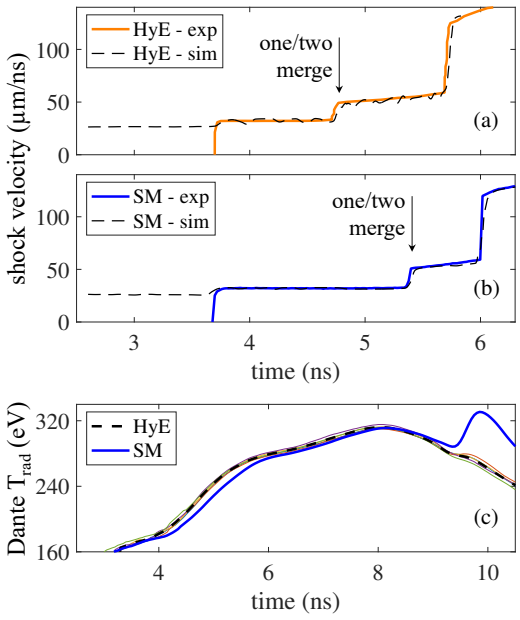

FIG. 4. (Color online) Experimental shock-timing measurements for (a) HyE and (b) SM confirm the one/two shock merge is delayed as designed with the updated SM pulse shape. (c) Temporally-resolved Dante-1 data further corroborate that the capsule drive for SM is delayed compared to HyE, as intended, while reaching the same peak radiation temperature. The peak at ∼9.5 ns is a signature of the high neutron yield, from reheating of the hohlraum by the expanding target following peak compression.

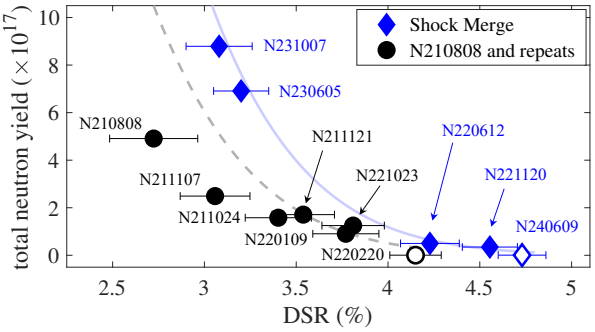

FIG. 5. (Color online) Total neutron yield as a function of DSR for the HyE (black circles) and SM (blue diamonds) experiments. DSR decreases with increasing yield for the same implosion design and for Y_{amp}¿1, as the neutron yield causes a rapid expansion of the hot spot during neutron emission. The design-specific peak DSR is therefore extracted from implosions using dudded THD fuel without yield amplification, shown as the open symbols. The solid (SM) and dashed (HyE) lines are calculated Y-vs-DSR curves from 1D simulations. The SM data show a clear enhancement in both yield and DSR compared to N210808 and its repeats, and better agreement with its characteristic curve.

ment. Of particular interest is the velocity jump from ∼30μm/ns to ∼50μm/ns around 5 ns, which is a signature of the one/two shock merge, and with the relative delay of this feature between SM and HyE being consistent with predictions. This confirms the intended shock timing for the updated SM pulse shape. Further evidence of the as-intended behavior is seen in Fig. 4(c), which shows the experimental, temporally-resolved radiation temperature, T_{rad}, as measured by the Dante diagnostic.[41] Note that Dante encountered a hardware problem on N210808, and did not produce data for that experiment . Instead, the dashed black line is the average temperature history from the series of N210808-repeat experiments, which are shown as the underlying thin, solid lines, and which exhibited excellent repeatability. The data for SM experiment N231007 (blue, solid line) exhibits the intended delay in its rise to peak power, but otherwise follows the same temperature history and reaches the same amplitude, thus maintaining the same capsule drive between the two designs. Note the large peak at 10 ns for N231007 in Fig. 4(c), a signature of the multi-MJ yield produced on the shot.[42] The igniting hot spot reaches pressures in excess of 100 Gbar, which causes a rapid explosion of the remaining fuel and shell after peak convergence. This recompresses the surrounding, expanded ablator material, and in the process causes significant heating of the surrounding hohlraum wall. It is this reheating that is seen in the blue curve in Fig. 4(c). Note that this is also visible in the collection of N210808-repeat curves, albeit at much lower amplitudes because of the lower yield on those experiments.

Figure 5 shows the key results from the SM campaign. It plots the experimentally measured, 4π-averaged downscatter ratio, DSR, as a function of the total neutron yield for the series of N210808-like experiments (black circles) and the SM series (blue diamonds). The shown data includes horizontal error bars, while the vertical error bars have been omitted for clarity. The yield uncertainty is of order 5% and is generally smaller than the extent of the data symbol. Crucially, the SM experiments reach both higher yields and DSR's, surpassing the previously best performing experiment with a 1.9-MJ laser drive, N210808. Additionally, Fig. 6 shows equatorial neutron imaging data (top row) and ΔDSR skymaps (bottom row) for the SM shots and a representative HyE experiment (N211107). Key experimental data, and fielding parameters for relevant experiments are discussed below in more detail and are also summarized in Table I.

Notably, for both the SM and HyE data groups in Fig. 5, the DSR decreases with increasing yield. For experiments with no or negligible yield amplification both yield and DSR scale with the energy coupled to the hot spot. In contrast, for implosions near the ignition cliff, and Y_{amp}>1, the pressure and temperature resulting from the increasing levels of α-heating and fusion yields, force a rapid explosion during neutron production, and a concurrent drop in ρR. The increasing hot-spot pressures at higher yields further accelerate the expansion, leading to a decrease of the neutron-emission–weighted areal den-

TABLE I. Key experimental parameters, target-quality metrics, and data for the SM campaign and select HyE experiments.

Shot ID	N210808	N220220	N220612	N221120	N230605	N231007	N240609
type	HyE	HyE	SM	SM	SM	SM	SM
fuel	DT	THD	DT	DT	DT	DT	THD
DT fuel age (hr)	125.4	-	152.1	130.8	162.5	151.1	-
layer thickness (μm)	65.9	65.9	66.0	66.6	65.6	65.0	64.5
laser energy (MJ)	1.92	1.94	1.90	1.88	1.88	1.89	1.88
$\Delta\lambda$ (Å)	1.8	1.8	2.0	2.5	2.7	2.7	2.7
capsule batch	KC789	KC789	KC930	KC931	KC1071	KC1071	KC1071
inner radius (μm)	1048.8	1048.8	1050.3	1050.3	1048.6	1048.6	1048.6
wall thickness (μm)	79.6	79.3	79.5	79.4	79.6	79.3	79.5
W dopant (at.%-μm)	8.5	8.3	9.2	9.3	8.0	8.0	7.8
capsule mode 1 (μm)	0.2	0.44	0.25	0.24	0.2	0.16	0.13
surface pits $< 1\mu m^3$	270	139	503	179	663	286	436
surface pits $\geq 1\mu m^3$	0	1	2	2	1	6	3
voids $< 10\mu m^3$	40	0	260	180	40	40	100
voids $\geq 10\mu m^3$	0	0	0	0	0	0	0
inclusions $<200\mu m^3$	22	28	207	220	12	30	28
inclusions $\geq 200\mu m^3$	3	4	20	9	1	0	4
surface particles $<100\mu m^3$	2	3	1	3	0	1	0
surface particles $\geq 100\mu m^3$	0	1	0	2	1	1	0
petal defects	no	no	yes	yes	no	no	no
Y_{total} ($\times 10^{16}$)	49±2	0.051±0.002	5.0±0.2	2.0±0.1	69±3	88±4	0.062±0.002
burn-up fraction (%)	1.9	-	0.2	0.1	2.6	3.3	-
G	0.7±0.1	-	0.073±0.007	0.030±0.003	1.0±0.1	1.3±0.1	-
DSR (%)	2.72±0.25	4.14±0.15	4.23±0.16	4.55±0.18	3.20±0.15	3.08±0.18	4.73±0.16
DSR_{max}-DSR_{min} (%)	0.9	1.6	1.3	2.5	0.8	1.1	2.1
neutron P_0 (μm)	55.4±3.0	31.0±3.4	39.0±12.0	32.9±0.6	59.6±1.9	65.4±2.5	33.5±2.0
neutron P_2 (%)	-4.1±0.6	13.8±6.6	-35.5±7.5	3.5±1.3	0.6±1.8	1.0±1.6	5.6±4.3

sities as Y_{amp} increases.[9] This leads to a design-specific curve in Y-vs-DSR, with the highest DSR achieved in a hydrodynamically equivalent experiment, but without any Y_{amp}. In Fig. 5, the characteristic Y-vs-DSR curve for SM is shifted to the right and to higher DSR's compared to the curve mapped out by the N210808-repeat series.

Experiment N210808, and the left-most data point in Fig. 5, is the best-performing experiment in the 1.9-MJ HyE campaign. It achieved a total yield of Y=(4.9±0.2)×10^{17} at a DSR of 2.72±0.25%, or 1.33±0.13 MJ with a target gain of G=0.69±0.07. Performance on its repeat experiments was impacted by unintentional variations in laser delivery, and hot-spot mix induced by capsule defects, and never surpassed that of N210808.[29] Importantly, despite these shot-to-shot variations and using a wide range of capsule qualities with targets from three different batches, the experiments in the 1.9-MJ HyE campaign all follow a characteristic, and design-specific Y-vs-DSR curve. Therefore, this well-studied design provides a robust baseline to compare against when introducing deliberate changes to the design adiabat, as with the SM experiments.

Four, DT-filled SM experiments were conducted in the series. The first two, N220612 and N221120, did exhibit increased DSR compared to the HyE series (see Fig. 5), albeit at a reduced yield of <5×10^{16}. Performance for these experiments was degraded by implosion asymmetry and capsule-quality induced mix. Most significantly, both shots experienced significant levels of mix as a result of *petal* defects, a localized density perturbation seeded by debris embedded in the capsule wall during the coating process. Additionally, as seen in Fig. 6(a), neutron-imaging data for N220612 show a >30% oblate hot spot, indicating an asymmetric capsule drive and an inefficient implosion. The longer SM pulse shape affects the capsule symmetry as it allows for further expansion of the hohlraum wall during the laser drive compared to HyE. This reduces laser beam propagation to the hohlraum waist via absorption in the wall plasma.[31–33] To offset this, experiment N220612 already used an increased wavelength separation between inner and outer beams of 2.0Å compared to 1.8Å for HyE, and for the follow-up shot, N221120, this was increased to 2.5Å. The larger $\Delta\lambda$ resulted in a near-round implosion with a ∼3% prolate hot spot, as can be seen in the neutron-imaging data in Fig. 6(b), indicating a balanced mode-2 drive. However, N221120 suffered from an unusually large mode-1

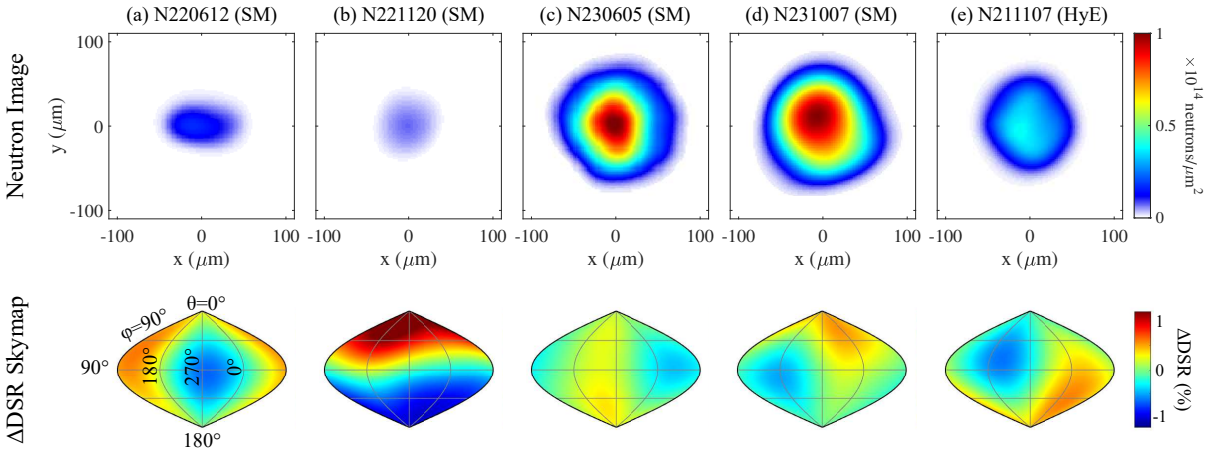

FIG. 6. (Color online) (top row) Neutron imaging data and (bottom row) ΔDSR skymaps for the series of SM experiment, and one representative HyE experiment, N211107. The first two SM shots, (a) N220612 and (b) N221120, suffered from significant drive asymmetry and reduced performance, while the other data exhibit only moderate asymmetry.

perturbation caused by a capsule-wall mode-1 co-aligned with adventitious laser asymmetry. This resulted in a highly asymmetric drive as evidenced by the DSR distribution shown in Fig. 6(b) and a value of (DSR_{max}-DSR_{min})/DSR≈60%. While the capsule quality, and in particular the petal defects, are believed to be the main source of performance degradation for both N220612, and N221120, both mode-1 and mode-2 asymmetries are known to be highly detrimental to performance.[43,44]

In contrast, the following experiments, N230605 and N231007, used much higher capsule-quality targets without any petal defects, and comparable in quality to the capsule used on N210808, see also Table I. Both experiments exhibited only moderate levels of mix or asymmetry (see Fig. 6). One more adjustment was applied to N230605 to account for a systematic, ∼8% underdelivery of the on-target laser energy in the foot up to ∼2 ns compared to the design goal. This led to a weaker-than-designed first shock, and a calculated shock merger depth of ∼7μm from the inner ice surface, and inside the ice layer, or roughly half way between N210808 and the intended merger point at the ice/ablator interface. Increasing the laser energy in the foot further required a small adjustment of the wavelength separation to its final value of 2.7Å to ensure implosion symmetry is maintained. These changes proved highly successful and shot N230605 achieved Y=(6.9±0.3)×10^{17} at a DSR of 3.20±0.15%, or a total yield of 1.91±0.19 MJ with a target gain of G=1.0±0.1. Following this success, no further design changes were implemented for the final DT-fueled experiment, N231007, which proved to be the best-performing one in the SM series. It achieved Y=(8.8±0.4)×10^{17}, DSR=3.08±0.18%, and 2.38±0.24 MJ or G=1.26±0.13, increasing the yield compared to the reference experiment, N210808, by almost 80%. Notably, the experimental fielding conditions and input parameters are highly comparable between N230605 and N231007, and well within typical shot-to-shot variability, and the ∼30% increase in fusion yield on the latter experiment is a reflection of the highly sensitive implosion dynamics near the ignition cliff. Either way, at the time of writing, N231007 is best-performing experiment with a drive laser of 1.9 MJ, and the only experiment to have achieved ignition and G>1 with a laser energy of less than 2.04 MJ.

It is worth emphasizing that the last two SM experiments used nearly identical fielding conditions and targets from a capsule batch of similar quality in all measured metrological values as that used on N210808. Of note, though, is the difference in fuel age used on the two high-performing SM experiments compared to that of N210808, with SM using somewhat older fuel than for the reference experiment. Fuel age refers to the time between the final ^{3}He purge from the DT used for creating the fuel layer, and the shot time. Helium-3 contamination is caused by beta decay of the tritium with a half life of 12.3 years, releasing ∼82 ng per 100 hours for the experiments discussed here. While fueling the target, the ^{3}He is mixed uniformly into the DT fuel. However, it is then released out of the fuel and trapped inside the central vapor volume during the formation of the DT-ice layer at 18.6K, as the boiling temperature of ^{3}He is 3.2K. This contamination of the central vapor gas can increase energy losses from radiation during the implosion, thus negatively affecting fusion performance. For that reason, the fuel age is typically limited to ∼100 to 150 hours to limit the buildup of ^{3}He contamination. Notably, this is expected to matter the most for experiments near the ignition cliff, where small changes to the hot spot conditions have a large impact on fusion performance.[7,10] Given the fuel age, the ^{3}He atomic-fraction in the hot spot of N210808 is calculated as 4.5%, compared to 6.4% on N230605 and 5.9% on N231007. In 1D calculations this lowers the total yield for the two SM experiments on

the order of 10% to 15% compared to N210808. However, as there is no direct measurement of the as-shot helium-3 concentration, its experimental impact remains difficult to quantify.

To confirm that SM does achieve higher compression compared to HyE, the DSR was measured for both implosion designs in the absence of α-particle heating using companion THD experiments. Here, the cryogenic fuel layer comprises a reduced deuterium fraction, while increasing protium (H) and tritium (T) content to reduce the fuel reactivity but maintain the same fuel mass and density, and thus its hydrodynamic properties.[12] The respective data for HyE (shot N220220)[45] and SM (N240609) are shown in Fig. 5 as the empty symbols, marking the lowest yield/highest DSR in each dataset, and giving DSR's of 4.14±0.15% (HyE) and 4.73±0.16% (SM), compared to the 1D-calculated values of 4.39% and 4.88%, respectively. Note that the experimental DSR values for the THD data have been corrected for degradation from mode-1 asymmetry using the piston model.[44,46,47] This estimates the degradation of an implosion because of shell asymmetry, by relating the non-uniformly distributed shell kinetic energy to the experimentally measured hot-spot drift velocity. It can be shown that the nominal DSR is degraded by a factor $(1 - f^2)$, where $f = v_{hs}/v_{imp}$, is the shell asymmetry fraction given by the ratio of the hot-spot drift velocity, v_{hs}, over the implosion velocity, v_{imp}. This relative correction of 3 to 5% is only applied to the low-yield data, as the underlying assumption of an adiabatic hot spot evolution with $PV^\gamma = const$ only holds for yield amplification levels of $\lesssim$1.[44] Uncorrected DSR's for the HyE and SM THD implosions are 4.03% and 4.48%, respectively. Including the mode-1 correction, the SM DSR increased compared to HyE by 14±6%, a clear enhancement in the relative compression well outside of the error bars. The relative change between the two designs is consistent with the relative change in the accompanying 1D simulations (11%). Notably, this is also the first demonstration that DSR and compression can be increased in HDC ablators by lowering the adiabat.[48] The calculated, design-characteristic Y-vs-DSR curves for both the HyE and SM experiments are also shown in Fig. 5 as the dashed, gray (HyE) and solid, blue (SM) lines, respectively. These curves were generated by artificially adjusting the multiplier for charged-particle stopping power in the simulations from 0 to 1, thereby suppressing Y_{amp} from α-particle deposition. This is necessarily an unphysical treatment, and ignores important multi-dimensional physics and degradation mechanisms. It does accurately capture the experimentally observed no-burn compression, as expected, but is otherwise primarily meant to illustrate the inverse relationship between yield and DSR in this yield range.

The THD data in Fig. 5 demonstrate that, given the same fuel mass and shell thickness, the SM design achieves a higher compression at minimum volume. It follows that for HyE and SM implosions that have the *same* measured DSR, the SM experiment is necessarily expected to exhibit a larger hot spot. This is consistent with the data in Fig. 6, when comparing the spatially resolved neutron emission for experiments N231007 (SM) and N211107 (HyE), Figs. 6(d) and (e), respectively. This is also shown in Fig. 7, which plots the respective angularly averaged profiles. With a nuclear yield of 2.0×10^{16}, N211107 is the second-best performing experiment in the HyE series, and features a DSR of 3.06±0.19%, matching the SM experiment N231007. As can be seen in both Figs. 6 and 7 the SM data exhibit both a brighter peak emission and a larger hot-spot radius compared to the HyE data (P_0=54 μm vs 65 μm), consistent with expectations and the reported differences in yield.[9]

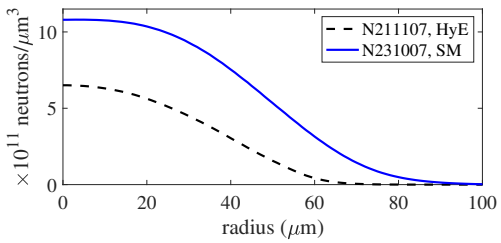

FIG. 7. (Color online) Radially averaged neutron-emission profiles for HyE experiment N211107 and SM shot N231007. Both the size and emission brightness are noticeably increased in the SM data, consistent with the observed, total neutron yield.

The combined data for the THD- and DT-fueled experiments definitively demonstrate the correlation between reduced adiabat, increased fuel compression, and improved ICF performance, thus answering a long-standing question. It is worth noting that these results were made possible only by recent advancements in ICF experiments and target manufacturing, enabling both N210808-like target quality and implosions in the ignition regime. Lowering the adiabat is only a strong lever in the burning plasma or ignition regime, as Eq. 1 otherwise reduces to the much weaker $Y\sim\rho R^{1.5}$, and small changes in density are easily masked by experimental shot-to-shot variability. Furthermore, higher design efficiency generally decreases robustness to instability growth, and thus sensitivity to imperfections in the capsule which can act as instability seeds. These instabilities can lead to interpenetration of fuel and ablator material, in turn leading to increases in radiative losses and premature cooling of the hot spot.[49] Indeed, this is thought to have caused the reduced performance on the SM experiments N220612 and N221120, where capsule quality and, in particular, the presence of petal defects in the capsule wall were of concern. An interesting point of comparison is the HyE experiment N221023, see Fig. 5. It also used a capsule with petal defects and from the same batch as N220612, and performed well below N210808 and most of its repeats. With a total yield of 1.2×10^{17} neutrons it is nearly the lowest performing experiment in the 1.9-MJ HyE series,

only marginally outperforming N220109 which achieved 0.9×10^{17}. Experiment N220109 did not have petal defects but in turn suffered from significant mix caused by other capsule inclusions and particle debris on the outer capsule wall, again showing high sensitivity of ICF performance to capsule quality.[29] It may be argued that the performance degradation on SM was more severe than on HyE, consistent with a higher expected sensitivity to perturbations owing to its lower design adiabat. This further emphasizes that it has only been through recent improvements in capsule metrology and identifying instability seeds, as well as refinements in target manufacturing to reduce both their prevalence and magnitude, that lower-adiabat implosions have become viable.

The experiments discussed here highlight the need to control instability growth in the pursuit of higher compression and increased ICF performance, and novel design approaches are being investigated to address current limitations. One example is the so-called *SQ-n* design, which replaces the traditional 3-shock pulse shape [see Fig. 2(a)] with a single, higher first shock, followed by a gently rising ramp to peak power. In calculations, this maintains a low adiabat, while significantly reducing the mix at the fuel-ablator interface.[50,51] The design also aims to mitigate mix from the inherently unstable doped/undoped interface inside the ablator. Replacing this step-profile design with either a continuous gradient dopant profile, or by extending the dopant layer to the inside capsule surface, has been shown to significantly improve experimentally measured compression. This has the potential to reach even higher DSR's than with the SM design, without incurring a mix penalty.[52] An experimental campaign to test these concepts on the NIF in the burning-plasma and ignition regimes is already underway.

IV. CONCLUSIONS

In summary, this study represents a significant breakthrough in ICF by conclusively demonstrating the potential of reduced adiabat designs to enhance fusion performance. For the first time, increased fusion yield has been achieved on the NIF through improved fuel compression via reducing the design adiabat. This was accomplished by making small adjustments to the laser pulse shape and the resulting shock timing, building on the previously best-performing 1.9 MJ laser-drive experiment, shot N210808. The ShockMerge design achieved an 80% increase in fusion yield and a 14% improvement in fuel compression compared to the baseline, with excellent repeatability. Additionally, THD implosions confirmed the enhanced compression, and experiment N231007 stands as the only experiment to achieve ignition and a target gain $G > 1$ using 1.9 MJ of laser energy. These results highlight the critical role of optimizing shock timing and fuel compression in overcoming current performance limitations, offering a promising pathway toward future ICF applications.

ACKNOWLEDGMENTS

The data that support the findings of this study are available from the corresponding author upon reasonable request. The authors would like to thank the NIF operations, laser, target fabrication, and diagnostic teams for their dedicated efforts during these experiments, and R. D. Petrasso for their valuable insights. This work was performed under the auspices of the U.S. Department of Energy by Lawrence Livermore National Laboratory under Contract DE-AC52-07NA27344. LLNL release number LLNL-JRNL-872936.

[1]G. H. Miller, E. I. Moses, and C. R. Wuest, Opt. Eng. **43**, 2841 (2004).
[2]J. Nuckolls, L. Wood, A. Thiessen, and G. Zimmerman, Nature **239**, 139 (1972).
[3]J. D. Lindl, *Inertial Confinement Fusion: The Quest for Ignition and Energy Gain Using Indirect Drive* (Springer-Verlag, New York, 1998).
[4]S. Atzeni and J. Meyer-ter Vehn, *The Physics of Inertial Fusion: Beam Plasma Interaction, Hydrodynamics, Hot Dense Matter*, International Series of Monographs on Physics (Clarendon Press, Oxford, 2004).
[5]H. Abu-Shawareb, R. Acree, P. Adams, J. Adams, B. Addis, R. Aden, P. Adrian, B. B. Afeyan, M. Aggleton, L. Aghaian *et al.*, Phys. Rev. Lett. **132**, 065102 (2024).
[6]O. L. Landen, R. C. Nora, J. D. Lindl, A. L. Kritcher, S. W. Haan, M. D. Rosen, A. Pak, L. Divol, K. L. Baker, P. A. Amendt, D. D.-M. Ho, J. L. Milovich, J. E. Ralph, D. S. Clark, K. D. Humbird, M. Hohenberger, C. R. Weber, R. Tommasini, D. T. Casey, C. V. Young, D. J. Schlossberg, S. A. Maclaren, E. L. Dewald, P. F. Schmit, T. Chapman, D. E. Hinkel, J. D. Moody, V. A. Smalyuk, O. A. Hurricane, and R. P. J. Town, Phys. Plasmas **31**, 062712 (2024).
[7]O. L. Landen, K. L. Baker, D. T. Casey, L. Divol, S. W. Haan, D. Ho, O. A. Hurricane , A. L. Kritcher , J. D. Lindl, S. A. MacLaren, R. C. Nora, A. Pak, J. Ralph, V. Smalyuk , R. Tommasini , C. Weber, *High Energy Density Phys* **52**, 101101 (2024).
[8]A. L. Kritcher, A. Zylstra, C. Weber, O. Hurricane, D. A. Callahan, D. S. Clark, L. Divol, D. E. Hinkel, K. Humbird, O. Jones et al., following paper, Design of the first fusion experiment to achieve target energy gain G>1, Phys. Rev. E 109, 025204 (2024).
[9]A. Pak, A. B. Zylstra, K. L. Baker, D. T. Casey, E. Dewald, L. Divol, M. Hohenberger, A. S. Moore, J. E. Ralph, D. J. Schlossberg, R. Tommasini, N. Aybar, B. Bachmann, R. M. Bionta, D. Fittinghoff, M. Gatu Johnson, H. Geppert Kleinrath, V. Geppert Kleinrath, K. D. Hahn, M. S. Rubery, O. L. Landen, J. D. Moody, L. Aghaian, A. Allen, S. H. Baxamusa, S. D. Bhandarkar, J. Biener, N. W. Birge, T. Braun, T. M. Briggs, C. Choate, D. S. Clark, J. W. Crippen, C. Danly, T. Döppner, M. Durocher, M. Erickson, T. Fehrenbach, M. Freeman, M. Havre, S. Hayes, T. Hilsabeck, J. P. Holder, K. D. Humbird, O. A. Hurricane, N. Izumi, S. M. Kerr, S. F. Khan, Y. H. Kim, C. Kong, J. Jeet, B. Kozioziemski, A. L. Kritcher, K. M. Lamb, N. C. Lemos, B. J. MacGowan, A. J. Mackinnon, A. G. MacPhee, E. V. Marley, K. Meaney, M. Millot, J.-M.G.DiNicola, A. Nikroo, R. Nora, M. Ratledge, J. S. Ross, S. J. Shin, V. A. Smalyuk, M. Stadermann, S. Stoupin, T. Suratwala, C. Trosseille, B. Van Wonterghem, C. R. Weber, C. Wild, C. Wilde, P. T. Wooddy, B. N. Woodworth, and C. V. Young, Phys. Rev. E **109**, 025203 (2024).
[10]S. W. Haan, J. D. Lindl, D. A. Callahan, D. S. Clark, J. D. Salmonson, B. A. Hammel, L. J. Atherton, R. C. Cook, M. J. Edwards, S. Glenzer, A. V. Hamza, S. P. Hatchett, M. C. Her-

rmann, D. E. Hinkel, D. D. Ho, H. Huang, O. S. Jones, J. Kline, G. Kyrala, O. L. Landen, B. J. MacGowan, M. M. Marinak, D. D. Meyerhofer, J. L. Milovich, K. A. Moreno, E. I. Moses, D. H. Munro, A. Nikroo, R. E. Olson, K. Peterson, S. M. Pollaine, J. E. Ralph, H. F. Robey, B. K. Spears, P. T. Springer, L. J. Suter, C. A. Thomas, R. P. Town, R. Vesey, S. V. Weber, H. L. Wilkens, and D. C. Wilson, Phys. Plasmas **18**, 051001 (2011).

[11]M.C. Herrmann, M. Tabak and J.D. Lindl, *Nucl. Fusion* 41, 99 (2001)

[12]M. J. Edwards, J. D. Lindl, B. K. Spears, S. V. Weber, L. J. Atherton, D. L. Bleuel, D. K. Bradley, D. A. Callahan, C. J. Cerjan, D Clark *et al.*, Phys. Plasmas 18, 051003 (2011).

[13]O. A. Hurricane, D. A. Callahan, P. T. Springer, M. J. Edwards, P. Patel, K. Baker, D. T. Casey, L. Divol, T. Döppner, D. E. Hinkel, L. F. Berzak Hopkins, A. Kritcher, S. Le Pape, S. Maclaren, L. Masse, A. Pak, L. Pickworth, J. Ralph, C. Thomas, A. Yi and A. Zylstra, Beyond alpha-heating: driving inertially confined fusion implosions toward a burning-plasma state on the National Ignition Facility, Plasma Phys. Control. Fusion **61**, 014033 (2019).

[14]H. F. Robey, V. A. Smalyuk, J. L. Milovich, T. Döppner, D. T. Casey, K. L. Baker, J. L. Peterson, B. Bachmann, L. F. Berzak Hopkins, E. Bond *et al.*, Phys. Plasmas 23, 056303 (2016).

[15]V. A. Smalyuk, H. F. Robey, T. Döppner, D. T. Casey, D. S. Clark , O. S. Jones, J. L. Milovich, J. L. Peterson, B. Bachmann, K. L. Baker *et al.* Phys. Plasmas 23, 102703 (2016).

[16]C. A. Thomas, E. M. Campbell, K. L. Baker, D. T. Casey, M. Hohenberger, A. L. Kritcher, B. K. Spears, S. F. Khan, R. Nora, D. T. Woods *et al.*, Phys. Plasmas 27, 112708 (2020).

[17]T. C. Sangster, V. N. Goncharov, R. Betti, P. B. Radha, T. R. Boehly, D. T. Casey, T. J. B. Collins, R. S. Craxton, J. A. Delettrez, D. H. Edgell *et al.*, Phys. Plasmas 20, 056317 (2013).

[18]S. Raman, V. A. Smalyuk, D. T. Casey, S. W. Haan, D. E. Hoover, O. A. Hurricane, J. J. Kroll, A. Nikroo, J. L. Peterson, B. A. Remington, H. F. Robey, D. S. Clark, B. A. Hammel, O. L. Landen, M. M. Marinak, D. H. Munro, K. J. Peterson, and J. Salmonson, Phys. Plasmas 21, 072710 (2014).

[19]A. Pak, L. Divol, C. R. Weber, L. F. Berzak Hopkins, D. S. Clark, E. L. Dewald, D. N. Fittinghoff, V. Geppert-Kleinrath, M. Hohenberger, S. Le Pape, T. Ma, A. G. MacPhee, D. A. Mariscal, E. Marley, A. S. Moore, L. A. Pickworth, P. L. Volegov, C. Wilde, O. A. Hurricane, and P. K. Patel, Impact of Localized Radiative Loss on Inertial Confinement Fusion Implosions, Phys. Rev. Lett. 124, 145001 (2020).

[20]B. Bachmann, J. E. Ralph, A. B. Zylstra, S. A. MacLaren, T. Döppner, D. O. Gericke, G. W. Collins, O. A. Hurricane, T. Ma, J. R. Rygg, H. A. Scott, S. A. Yi, and P. K. Patel, Localized mix-induced radiative cooling in a capsule implosion at the National Ignition Facility, Phys. Rev. E 101, 033205 (2020).

[21]A. B. Zylstra, D. T. Casey, A. Kritcher, L. Pickworth, B. Bachmann, K. Baker, J. Biener, T. Braun, D. Clark, V. Geppert-Kleinrath, M. Hohenberger, C. Kong, S. Le Pape, A. Nikroo, N. Rice, M. Rubery, M. Stadermann, D. Strozzi, C. Thomas, P. Volegov, C. Weber, C. Wild, C. Wilde, D. A. Callahan, and O. A. Hurricane, Hot-spot mix in large-scale HDC implosions at NIF, Phys. Plasmas 27, 092709 (2020).

[22]D. S. Clark, A. Allen, S. H. Baxamusa, J. Biener, M. M. Biener, T. Braun, S. Davidovits, L. Divol, W. A. Farmer, T. Fehrenbach, C. Kong, M. Millot, J. Milovich, A. Nikroo, R. C. Nora, A. E. Pak, M. S. Rubery, M. Stadermann, P. Sterne, C. R. Weber, and C. Wild, Modeling ablator defects as a source of mix in high-performance implosions at the National Ignition Facility, Phys. Plasmas 31, 062706 (2024).

[23]T. Döppner, D. A. Callahan, O. A. Hurricane, D. E. Hinkel, T. Ma, H.-S. Park, L. F. Berzak Hopkins, D. T. Casey, P. Celliers, E. L. Dewald *et al.*, Phys. Rev. Lett. 115, 055001 (2015)

[24]T. R. Dittrich, O. A. Hurricane, D. A. Callahan, E. L. Dewald, T. Döppner, D. E. Hinkel, L. F. Berzak Hopkins, S. Le Pape, T. Ma, J. L. Milovich, J. C. Moreno, P. K. Patel, H.-S. Park, B. A. Remington, and J. D. Salmonson, Phys. Rev. Lett. 112, 055002 (2014) .

[25]V. Gopalaswamy, R. Betti, J. P. Knauer, N. Luciani, D. Patel, K. M. Woo, A. Bose, I. V. Igumenshchev, E. M. Campbell, K. S. Anderson *et al*, Nature 565, 581 (2019)

[26]H. Abu-Shawareb, R. Acree, P. Adams, J. Adams, B. Addis, R. Aden, P. Adrian, B. B. Afeyan, M. Aggleton, L. Aghaian *et al.*, Phys. Rev. Lett. **129**, 075001 (2022)

[27]A. L. Kritcher, A. B. Zylstra, D. A. Callahan, O. A. Hurricane, C. R. Weber, D. S. Clark, C. V. Young, J. E. Ralph, D. T. Casey, A. Pak *et al.*, Phys. Rev. E **106**, 025201 (2022).

[28]A. B. Zylstra, A. L. Kritcher, O. A. Hurricane, D. A. Callahan, J. E. Ralph, D. T. Casey, A. Pak, O. L. Landen, B. Bachmann, K. L. Baker *et al.*, Phys. Rev. E **106**, 025202 (2022).

[29]L. Divol, A. Pak, B. Bachmann, K. L. Baker, S. Baxamusa, J. Biener, R. Bionta, T. Braun, D. T. Casey, C. Choate *et al.*, Phys. Plasmas **31**, 102703 (2024)

[30]M. M. Marinak, G. D. Kerbel, N. A. Gentile, O. Jones, D. Munro, S. Pollaine, T. R. Dittrich, S. W. Haan, Three-dimensional HYDRA simulations of National Ignition Facility targets, Phys. Plasmas 8, 2275 (2001).

[31]D. A. Callahan, O. A. Hurricane, J. E. Ralph, C. A. Thomas, K. L. Baker, L. R. Benedetti, L. F. Berzak Hopkins, D. T. Casey, T. Chapman, C. E. Czajka, E. L. Dewald, L. Divol, T. Döppner, D. E. Hinkel, M. Hohenberger, L. C. Jarrott, S. F. Khan, A. L. Kritcher, O. L. Landen, S. LePape, S. A. MacLaren, L. P. Masse, N. B. Meezan, A. E. Pak, J. D. Salmonson, D. T. Woods, N. Izumi, T. Ma, D. A. Mariscal, S. R. Nagel, J. L. Kline, G. A. Kyrala, E. N. Loomis, S. A. Yi, A. B. Zylstra, and S. H. Batha, Phys. Plasmas 25, 056305 (2018).

[32]J. E. Ralph, O. Landen, L. Divol, A. Pak, T. Ma, D. A. Callahan, A. L. Kritcher, T. D€oppner, D. E. Hinkel, C. Jarrott, J. D. Moody, B. B. Pollock, O. Hurricane, and M. J. Edwards, Phys. Plasmas 25, 082701 (2018).

[33]M. Hohenberger, D. T. Casey, C. A. Thomas, O. L. Landen, K. L. Baker, L. R. Benedetti, D. A. Callahan, O. A. Hurricane, N. Izumi, S. F. Khan, T. Ma, D. A. Mariscal, S. R. Nagel, A. Pak, and B. K. Spears, Phys. Plasmas 26, 112707 (2019).

[34]P. Michel, L. Divol, E. A. Williams, S. Weber, C. A. Thomas, D. A. Callahan, S. W. Haan, J. D. Salmonson, S. Dixit, D. E. Hinkel, M. J. Edwards, B. J. MacGowan, J. D. Lindl, S. H. Glenzer, and L. J. Suter, Tuning the implosion symmetry of ICF targets via controlled crossed-beam energy transfer, Phys. Rev. Lett. 102, 025004 (2009).

[35]J.A. Frenje, R. Bionta, E. J. Bond, J. A. Caggiano, D. T. Casey, C. Cerjan, J. Edwards, M. Eckart, D. N. Fittinghoff, S. Friedrich *et al.*, Nucl. Fusion **53** 043014 (2013).

[36]A. R. Christopherson, O. A. Hurricane, C. Weber, A. Kritcher, R. Nora, J. Salmonson, R. Tran, J. Milovich, S. Maclaren, D. Hinkel, and R. Betti, Phys. Plasmas 30, 062705 (2023).

[37]D. T. Casey, *et al.*, Three dimensional low-mode areal-density non-uniformities in indirect-drive implosions at the National Ignition Facility, Phys. Plasmas 28, 042708 (2021).

[38]D. H. Munro, P. M. Celliers, G. W. Collins, D. M. Gold, L. B. Da Silva, S. W. Haan, R. C. Cauble, B. A. Hammel, and W. W. Hsing, Shock timing technique for the National Ignition Facility, Phys. Plasmas **8**, 2245 (2001)

[39]P. M. Celliers, G. W. Collins, L. B. Da Silva, D. M. Gold, R. Cauble, R. J. Wallace, M. E. Foord, and B. A. Hammel, Phys. Rev. Lett. 84, 5564 (2000).

[40]P. M. Celliers, D. K. Bradley, G. W. Collins, D. G. Hicks, T. R. Boehly, W. J. Armstrong, Rev. Sci. Instrum. 75, 4916 (2004).

[41]M. S. Rubery, G. E. Kemp, M. C. Jones, N. Pelepchan, W. C. Stolte, and J. Heinmiller, *Rev. Sci. Instrum.* 94, 031101 (2023)

[42]M. S. Rubery, M. D. Rosen, N. Aybar, O. L. Landen, L. Divol, C. V. Young, C. Weber, J. Hammer, J. D. Moody, A. S. Moore, A. L. Kritcher, A. B. Zylstra, O. Hurricane, A. E. Pak, S. MacLaren, G. Zimmerman, J. Harte, and T. Woods, Phys. Rev. Lett. **132**, 065104 (2024)

[43]J. E. Ralph, J. S. Ross, A. B. Zylstra, A. L. Kritcher, H. F. Robey, C. V. Young, O. A. Hurricane, A. Pak, D. A. Callahan,

K. L. Baker *et al.*, Nature Comm. 15, 2975 (2024)
[44]D. T. Casey, B. J. MacGowan, J. D. Sater, A. B. Zylstra, O. L. Landen, J. Milovich, O. A. Hurricane, A. L. Kritcher, M. Hohenberger, K. Baker *et al.*, Phys. Rev. Lett. 126, 025002 (2021)
[45]A. R. Christopherson, D. Schlossberg, S. MacLaren, C. Weber, A. Zylstra, O. A. Hurricane, A. Kritcher, D. Hinkel, B. K. Spears, A. Pak *et al.*, Phys. Plasmas 31, 072709 (2024).
[46]O. A. Hurricane, D. T. Casey, O. Landen, A. L. Kritcher, R. Nora, P. K. Patel, J. A. Gaffney, K. D. Humbird, J. E. Field, M. K. G. Kruse, J. L. Peterson, B. K. Spears, An analytic asymmetric-piston model for the impact of mode-1 shell asymmetry on ICF implosions, Phys. Plasmas 27, 062704 (2020)
[47]O. A. Hurricane, D. T. Casey, O. Landen, D. A. Callahan, R. Bionta, S. Haan, A. L. Kritcher, R. Nora, P. K. Patel, P. T. Springer, and A. Zylstra, Extensions of a classical mechanics "piston-model" for understanding the impact of asymmetry on ICF implosions: The cases of mode 2, mode 2/1 coupling, time-dependent asymmetry, and the relationship to coast-time, Phys. Plasmas 29, 012703 (2022).
[48]O. L. Landen, J. D. Lindl, S. W. Haan, D. T. Casey, P. M. Celliers, D. N. Fittinghoff, N. Gharibyan, V. N. Goncharov, G. P. Grim, E. P. Hartouni *et al.*, Phys. Plasmas 28, 042705 (2021).
[49]B. Bachmann, *et al.*, Direct Experimental Proof of the Principal Role of Reduced High-Mode Hydrodynamic Mix in Recent Ignition Success on NIF, Phys. Rev. Lett. 135, 065101 (2025)
[50]D. S. Clark, D. T. Casey, C. R. Weber, O. S. Jones, K. L. Baker, E. L. Dewald, L. Divol, A. Do, A. L. Kritcher, O. L. Landen, M. Millot, J. L. Milovich, V. A. Smalyuk, D. J. Strozzi, A. E. Pak, R. Tommasini, and M. J. Edwards, Phys. Plasmas 29, 052710 (2022).
[51]R. Tommasini, D.T. Casey, D. Clark, A. Do, K.L. Baker, O.L. Landen, V.A. Smalyuk, C. Weber, B. Bachmann, E. Hartouni, S. Kerr, C. Krauland, E.V. Marley, M. Mil- lot, J. Milovich, R.C. Nora, A.E. Pak, D. Schlossberg, B. Woodworth, T.M. Briggs, D.M. Holunga, A. Nikroo, and M. Stadermann, Increased compression in hdc- based ablator implosions using modified drive profile, Phys. Rev. Research 5, L042034 (2023).
[52]R. Tommasini, D.T. Casey, D. Clark, A. Do, K.L. Baker, O.L. Landen, V.A. Smalyuk, C. Weber, B. Bachmann, E. Hartouni, S. Kerr, S. Khan, C. Krauland, A. L. Kritcher, E.V. Marley, M. Millot, J. Milovich, R.C. Nora, A.E. Pak, D. Schlossberg, D. J. Strozzi, B. Woodworth, A. Allen, S. H. Baxamusa, T.M. Briggs, T. Fehrenback, D.M. Holunga, A. Nikroo, C. Kong, C. Wild, M. Stadermann, High-compression implosions based on high density carbon ablator using modified drive and capsule dopant profiles, Phys. Plasmas 32, 032707 (2025).